Quantitative ultrasound characterization of locally advanced breast cancer by estimation of its scatterer properties

Hadi Tadayyon, Ali Sadeghi-Naini, Lauren Wirtzfeld, Frances C. Wright, and Gregory Czarnota

Articles you may be interested in

Multiparametric 3D in vivo ultrasound vibroelastography imaging of prostate cancer: Preliminary results
Med. Phys. **41**, 073505 (2014); 10.1118/1.4884226

Computer-aided classification of breast masses using speckle features of automated breast ultrasound images
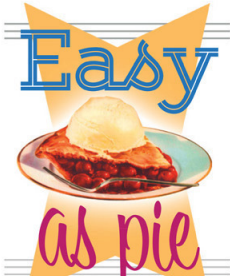Med. Phys. **39**, 6465 (2012); 10.1118/1.4754801

Development of a fully automatic scheme for detection of masses in whole breast ultrasound images
Med. Phys. **34**, 4378 (2007); 10.1118/1.2795825

Computerized-aid diagnosis of breast mass using ultrasound image
Med. Phys. **34**, 3158 (2007); 10.1118/1.2748112

Computerized characterization of breast masses on three-dimensional ultrasound volumes
Med. Phys. **31**, 744 (2004); 10.1118/1.1649531

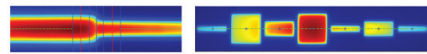# Quantitative ultrasound characterization of locally advanced breast cancer by estimation of its scatterer properties

Hadi Tadayyon
Physical Sciences, Sunnybrook Research Institute, Sunnybrook Health Sciences Centre, Toronto, Ontario M4N 3M5, Canada and Department of Medical Biophysics, Faculty of Medicine, University of Toronto, Toronto, Ontario M5G 2M9, Canada

Ali Sadeghi-Naini
Physical Sciences, Sunnybrook Research Institute, Sunnybrook Health Sciences Centre, Toronto, Ontario M4N 3M5, Canada; Department of Medical Biophysics, Faculty of Medicine, University of Toronto, Toronto, Ontario M5G 2M9, Canada; Department of Radiation Oncology, Odette Cancer Centre, Sunnybrook Health Sciences Centre, Toronto, Ontario M4N 3M5, Canada; and Department of Radiation Oncology, Faculty of Medicine, University of Toronto, Toronto, Ontario M5T 1P5, Canada

Lauren Wirtzfeld
Department of Physics, Ryerson University, Toronto, Ontario M5B 2K3, Canada

Frances C. Wright
Division of Surgical Oncology, Sunnybrook Health Sciences Centre, Toronto, Ontario M4N 3M5, Canada

Gregory Czarnota[a]
Physical Sciences, Sunnybrook Research Institute, Sunnybrook Health Sciences Centre, Toronto, Ontario M4N 3M5, Canada; Department of Medical Biophysics, Faculty of Medicine, University of Toronto, Toronto, Ontario M5G 2M9, Canada; Department of Radiation Oncology, Odette Cancer Centre, Sunnybrook Health Sciences Centre, Toronto, Ontario M4N 3M5, Canada; and Department of Radiation Oncology, Faculty of Medicine, University of Toronto, Toronto, Ontario M5T 1P5, Canada

Purpose: Tumor grading is an important part of breast cancer diagnosis and currently requires biopsy as its standard. Here, the authors investigate quantitative ultrasound parameters in locally advanced breast cancers that can potentially separate tumors from normal breast tissue and differentiate tumor grades.

Methods: Ultrasound images and radiofrequency data from 42 locally advanced breast cancer patients were acquired and analyzed. Parameters related to the linear regression of the power spectrum—midband fit, slope, and 0-MHz-intercept—were determined from breast tumors and normal breast tissues. Mean scatterer spacing was estimated from the spectral autocorrelation, and the effective scatterer diameter and effective acoustic concentration were estimated from the Gaussian form factor. Parametric maps of each quantitative ultrasound parameter were constructed from the gated radiofrequency segments in tumor and normal tissue regions of interest. In addition to the mean values of the parametric maps, higher order statistical features, computed from gray-level co-occurrence matrices were also determined and used for characterization. Finally, linear and quadratic discriminant analyses were performed using combinations of quantitative ultrasound parameters to classify breast tissues.

Results: Quantitative ultrasound parameters were found to be statistically different between tumor and normal tissue ($p < 0.05$). The combination of effective acoustic concentration and mean scatterer spacing could separate tumor from normal tissue with 82% accuracy, while the addition of effective scatterer diameter to the combination did not provide significant improvement (83% accuracy). Furthermore, the two advanced parameters, including effective scatterer diameter and mean scatterer spacing, were found to be statistically differentiating among grade I, II, and III tumors ($p = 0.014$ for scatterer spacing, $p = 0.035$ for effective scatterer diameter). The separation of the tumor grades further improved when the textural features of the effective scatterer diameter parametric map were combined with the mean value of the map ($p = 0.004$).

Conclusions: Overall, the binary classification results (tumor versus normal tissue) were more promising than tumor grade assessment. Combinations of advanced parameters can further improve the separation of tumors from normal tissue compared to the use of linear regression parameters. While the linear regression parameters were sufficient for characterizing breast tumors and normal breast tissues, advanced parameters and their textural features were required to better characterize tumor subtypes. © *2014 American Association of Physicists in Medicine.*
[http://dx.doi.org/10.1118/1.4852875]

1. INTRODUCTION

Breast cancer remains to be a clinical challenge given its prevalence and propensity to metastasize. Despite management efforts using systemic chemotherapy, surgery, and radiation therapy, an estimated 5-year survival rate of 55% was reported in the United States in 2004 for aggressive diseases.[1] Histologically determined tumor grade, one score indicating the degree of tumor aggressiveness, is a critical component of breast cancer diagnosis and plays a key role in planning an optimal treatment strategy for an individual patient. Tumor grade is highly recommended by the World Health Organization to be included in surgical pathology reports for invasive carcinoma.[2] Currently, the gold standard method of tumor grade determination is pathological examination of core biopsy specimens. However, not only can invasive core biopsies cause complications, including bleeding and infection, but approximately 10% of lesions require repeat biopsy due to sampling errors that occur during the initial biopsy.[3] Ultrasound (US) based characterization of tumors, if performed with high sensitivity and specificity, can serve as a noninvasive alternative to biopsies. Breast tumors larger than 8 mm are readily detected by clinical US scanners typically as hypoechoic regions.[4] Unfortunately, B-mode US images, which are used by radiologists for breast examination, do not readily identify frequency specific information, and lack otherwise available information about microstructural properties of tissues.[5] Quantitative ultrasound (QUS), which is a technique that analyzes the frequency dependence of the tissue backscatter signal, reveals information about the tissue's underlying microstructure, enabling the differentiation of disease from nondisease, and potential characterization of a disease into its subtypes.[6] As the grade of a tumor is linked to its microstructural properties (i.e., cellular organization), analysis of the frequency-dependence of the tumor backscatter could also reveal information about the tumor grade. Here, we present a QUS technique for the characterization of *in vivo* clinical breast tumors and surrounding normal tissue, and differentiation of tumor grades, using a conventional-frequency diagnostic ultrasound scanner.

Quantitative ultrasound encompasses a wide spectrum of tissue characterization techniques. For example, effective scatterer size and acoustic concentration have been used previously to differentiate mouse models of tumors from rat models of spontaneously occurring benign masses.[5] Effective scatterer diameter (ESD) and effective acoustic concentration (EAC) can be estimated by fitting a theoretical backscatter model to the measured backscatter signal from the tissue of interest. Previous studies found similarities between ESDs and the mean size of cancer cells (carcinoma and sarcoma) and glandular acini (fibroadenoma) which allowed tumors in mice to be differentiated from fibroadenomas in rats.[5] The tissue types were found to be better differentiated when the ESD and EAC parameters were combined. Moreover, these parameters were proven to be useful also in differentiating mouse carcinoma from sarcoma.[7] More recently, attempts were made in a clinical setting at differentiating malignant breast masses from their benign counterpart using QUS features such as ESD, heterogeneity index (standard deviation of ESD), and acoustic attenuation.[8] A considerable overlap was found in the backscatter and attenuation properties of the two mass types. Alternatively, tissue characterization parameters such as midband fit (MBF), spectral slope (SS), and spectral intercept (SI), can be obtained by a linear regression of the tissue power spectrum. By modeling the tissue echo power spectrum as a linear approximation of the acoustic impedance autocorrelation, Lizzi *et al.*[9] demonstrated that the spectral slope is related to the scatterer size and the intercept can be related to the scatterer concentration. These parameters of interest are estimated from a linear regression analysis of the tissue power spectrum within the usable bandwidth (usually corresponding to −6 dB range), representing the slope (SS) and intercept (SI) of the line, as well as the value of the fit at the center of the frequency bandwidth (MBF). These parameters have been investigated as a tool for the characterization of diseases in various types of tissues including prostate, lymph nodes, ocular tumors, as well as cardiac abnormalities,[10–13] and have also been used to characterize therapeutic effects such as tumor response to radiotherapy, antivascular, and hyperthermia treatments.[14–16] Another important, but as yet less frequently used parameter for tissue characterization, is the spacing among scatterers (SAS). The SAS parameter has proven to be effective for characterizing diffuse liver disease[17–20] and breast cancer.[21] Several methods have been used to estimate SAS, including the cepstrum,[22] wavelet transform,[23,24] and spectral autocorrelation (SAC) methods.[25] All methods involve the detection of the periodicity of a power spectrum, from which the spacing between quasiregular scatterers can be determined.

To date, the core of work on QUS characterization of breast cancer lies within the context of differentiating benign versus malignant tumors.[5,21,26] Tumor grade, however, has not been characterized by QUS to date, though certain sonographic features have been identified that correlate with tumor grade. For instance, in a study by Kim *et al.*,[27] lack of circumscribed margins, abrupt boundaries, and hypoechoic or complex echo patterns were more frequently observed in grade III invasive tumors compared to grade I and II invasive tumors. These subjectively interpreted features, however, require manual identification by trained radiologists, and thus these methods are prone to interuser variability in margin delineation and feature identification. On the other hand, QUS can provide less user-dependent and more quantitative information about the tumor grade. In this paper, we investigate the potential of six parameters—MBF, SS, SI, SAS, ESD, and EAC—to distinguish advanced breast tumors from their surrounding normal tissue and characterize their frequency-dependent properties in order to potentially differentiate between tumor grades.

2. MATERIALS AND METHODS

2.A. Ultrasound data acquisition and processing

The subjects in this study were comprised of 42 patients diagnosed with locally advanced breast cancer (LABC) of primarily invasive ductal carcinoma type. Subjects were

TABLE I. Patient characteristics. ER is estrogen receptor, PR is progesterone receptor, HER2 is the human epithelial growth factor receptor 2, IDC is invasive ductal carcinoma, and IMC is invasive micropapillary carcinoma. Tumor size refers to the longest diameter of the tumor.

Patient	Age	Tumor size (cm)	Grade	ER	PR	HER2	Type
1	55	8	I	−	+	+	IDC
2	53	9	II	+	+	−	IDC
3	41	4	III	+	+	+	IDC
4	65	10	II	−	−	−	IDC
5	50	5	III	+	+	+	IDC
6	33	3	I	+	+	−	IDC
7	46	8	III	−	−	−	IDC
8	41	9.7	II	+	+	+	IDC
9	48	4.9+3.2	II	+	+	−	IDC
10	36	5.8	II	+	+	−	IDC
11	40	4.4	III	−	−	−	IDC
12	62	14	III	−	−	−	IDC
13	59	6	II	−	−	−	IDC
14	65	6.7	II	+	−	−	IDC
15	38	9.2	II	+	+	−	IDC
16	53	12.7	III	−	−	−	IDC
17	48	9	II	+	+	+	IDC
18	50	13	III	−	−	−	IDC
19	49	8.9	III	−	−	+	IDC
20	46	15	III	−	−	−	IDC
21	40	3	III	−	+	+	IDC
22	56	3.2	II	−	−	+	IDC
23	49	2.8	III	−	−	+	IDC
24	47	5.2	II	+	+	−	IDC
25	52	4.1	II	+	+	−	IDC
26	44	9.9	II	+	+	+	IDC
27	38	2.2	II	+	+	−	IDC
28	58	1.9	III	−	+	−	IDC
29	36	12	I	+	+	−	IDC
30	37	N/A	III	+	+	−	IDC
31	38	8.8	III	+	+	+	IDC
32	73	7.6	III	+	+	+	IDC
33	47	12.5	II	+	+	−	IDC
34	57	7.9	III	−	−	−	IDC
35	53	4.7	II	+	+	−	IDC
36	56	2.2	II	+	+	−	IDC
37	84	4.7	II	−	−	−	IDC
38	33	10	III	+	+	+	IMC
39	39	3	III	−	−	−	IDC
40	45	6	I	+	+	+	IDC
41	60	N/A	II	+	−	+	IDC
42	45	3.8	II	+	+	−	IDC

recruited on a voluntary basis in an ongoing clinical trial at Sunnybrook Health Sciences Centre, Toronto, Canada. Table I presents the patient characteristics, including patient age, tumor size, grade, receptor status, and tumor type. For this study, patient data were divided into three groups: patients having grade I (four cases), II (19 cases), or III tumor (19 cases). Pathology data were obtained from biopsy specimens and confirmatory mastectomy specimens after surgery. Tumor grading was performed by institutional pathologists using a scheme modified from Bloom and Richardson.[28]

Ultrasound data were obtained using a Sonix RP clinical system equipped with a linear array transducer having a center frequency of 6 MHz and a −6 dB bandwidth of 4–7 MHz (L14-5/60, Ultrasonix, Vancouver, Canada). RF data were sampled at 40 MHz at 512 line density, resulting in images with 6 cm width and 4–6 cm depth. Four to seven image planes were selected at 1 cm intervals across the involved breast, with the transducer focus set at the midline of the tumor. These data provided typically four to six cross-sectional images of the tumor and one image of normal breast tissue. Although the majority of the tumors were readily visible in US scans, clinically obtained dynamic contrast-enhanced MR images of the patients were also available for cross-verification of approximate tumor location and morphology.

For QUS analysis, a rectangular region of interest (ROI) was defined in the center of the tumor cross section, ranging in size from 0.5 to 5 cm, depending on the tumor size. For the normal tissue image, a comparably sized ROI was defined. The ROIs for normal tissues were selected below the subcutaneous fat layer and generally contained glandular tissue (ducts and lobules). The six QUS parameters, MBF, SS, SI, SAS, ESD, and EAC, were computed from each ROI by analyzing the frequency dependence of the backscattered RF signal on a window by window basis. Square windows (5 × 5 mm) were selected in each ROI with 80% overlap between adjacent windows in both axial and lateral directions. This resulted in a spatial map of each QUS parameter, which is referred to as a parametric map. The size of the window was selected to cover approximately 17 wavelengths (∼5 mm), larger than the minimum size required to obtain reliable spectral parameters which are independent of window length (ten wavelengths).[29] In order to make the analysis method system-independent, the processed data were normalized to reference data. For linear regression power spectral analysis, a tissue-mimicking phantom constructed inhouse was used, comprising of agar gel embedded with glass microspheres, modified from Ref. 30. The phantom had an attenuation coefficient of 0.15 dB/cm/MHz and a BSC slope of 0.73 dB/Sr/cm/MHz. The methods used to obtain the above parameters will be explained in Sec. 2.D. For SAS analysis, spectral normalization was performed using a planar reflector reference spectrum. The reason for the choice of a planar reflector as reference was that the SAS parameter is highly sensitive to the spatial distribution of the scatterers in the reference medium. As such, a planar reflector would serve as a more appropriate reference since it does not possess the relatively complex scattering properties of the reference phantom.

2.B. Linear regression analysis of the normalized power spectrum

Linear regression analysis of the normalized power spectrum was based on a linear approximation of the Gaussian form factor model of tissue backscatter, proposed by Lizzi et al.[14] Defining a Hanning-gated RF echo segment as a function of time and lateral position as $e_s(t, x_i)$, the mean power spectrum from each window was estimated by taking

the square magnitude of the Fast Fourier transform (FFT) of $e_s(t, x_i)$, and averaging the result across RF lines $i = M, M + 1, \ldots, N$ in the window. In order to remove system-dependent effects, the power spectrum was normalized using the power spectrum obtained from a reference phantom echo, $e_p(t, x_i)$, in the corresponding location. This process is expressed by Eq. (1),

$$S(f) = \frac{\sum_{i=M}^{N} |\text{FFT}(e_s(t, x_i))|^2}{\sum_{i=M}^{N} |\text{FFT}(e_p(t, x_i))|^2}. \tag{1}$$

A line of best fit, using least squares, was found for the normalized power spectrum within the -6 dB frequency bandwidth as per Lizzi's method,[9]

$$S(f) = \text{SS} f + \text{SI}, \tag{2}$$

$$\text{MBF} = S(f_c), \tag{3}$$

where SS and SI are the slope and interpolated 0-MHz intercept of the line of best fit, and MBF is the solution of the line-approximated power spectrum at the center of the frequency bandwidth (i.e., 5.5 MHz). The bandwidth was determined from the power spectrum of a reference phantom.

2.C. Spectral autocorrelation and SAS

The mean SAS of our breast tumor data was estimated by computing the autocorrelation of the power spectrum estimated by the autoregressive (AR) model. This method has been demonstrated to detect distance between coherent scatterers in tissue microstructures having lower orders of regularity.[25] The AR model predicts the output of a stationary stochastic process as a linear combination of previous samples of its output, and was defined as[31]

$$\hat{e}_S[t] = \sum_{k=1}^{p} a_k \hat{e}_s[t - k] + w[t], \tag{4}$$

where a_k are the AR coefficients, $w[t]$ is a white noise input sequence, and p is the order of the AR model. The power spectrum, $|X(f)|^2$, can be obtained by Fourier transforming both sides of Eq. (4) to yield[21]

$$|X(f)^2| = \frac{2}{|1 + \sum_{k=1}^{p} a_k e^{-j2\pi fk}|^2}, \tag{5}$$

where δ is the standard deviation of the white noise. As demonstrated in Eq. (6), the normalized power spectrum, $S(f)$, was obtained in a manner similar to Sec. 2.B, except that the numerator was an AR-estimated power spectrum ($|X(f)|^2$) and the denominator was echo data from a polished Plexiglas surface, $e_r(t_n)$. The subscript "n" represents discrete depth intervals $n = 1, 2, \ldots, 6$ cm. Also $e_r(t_n)$ was independent of lateral location, x_i, as the power spectra of the reflector echoes were averaged across the RF lines over the image width to obtain a smooth mean power spectrum. This was done to obtain a good signal to noise ratio and to average out any microscopic variances in the planar reflector's surface

$$S(f, x_1) = \frac{\sum_{i=N}^{M} |X(f, x_i)|^2}{\sum_{i=0}^{L} |\text{FFT}(e_r(t_n))|^2}, \quad n = 1, 2, \ldots, 6 \text{ cm.} \tag{6}$$

Finally, the autocorrelation of the normalized AR power spectrum, $R_{ff}(\Delta f)$, was computed using Eq. (7),

$$R_{\text{ff}}(\Delta f) = \sum_{\Delta f=1}^{N} S(f)S(f - \Delta f), \tag{7}$$

which is termed the SAC. The SAS corresponded to the frequency lag, Δf_p, at which the first peak in the SAC occurs

$$\text{SAS} = \frac{c}{2\Delta f_p}, \tag{8}$$

where c is the mean speed of sound in the tissue of interest. For normal tissue ROIs, which encompassed mainly glandular tissue, a speed of sound of 1455 m/s was assumed while for tumor ROIs, a speed of sound of 1540 m/s was assumed. These values are consistent with tomography measurements of speed of sound in the breast.[32]

2.D. Backscatter coefficient (BSC) estimation and the Gaussian form factor

The BSC is defined as the differential backscattering cross-section per unit volume[33] and was calculated as follows:[34]

$$\hat{\sigma}_{\text{bs}}(f) = S(f)\sigma_{\text{br}}(f)e^{4(\alpha_s - \alpha_r)(R + \frac{\Delta z}{2})}, \tag{9}$$

where subscripts s and r denote sample and reference (phantom), respectively, α is the attenuation coefficient, Δz is the gate length, R is the distance between the transducer and the proximal surface of the gate. The BSC of the reference phantom (σ_{br}) was estimated using Eq. (9), by setting it as the sample and setting the reference as another phantom which was previously characterized by Anderson *et al.*[35] The reference phantom used here contained monodisperse glass microspheres of diameter 20 ± 3 μm. These acted as Rayleigh scatterers as they are much smaller than the wavelength of the interrogating ultrasound pulse (approximately 250 μm) and therefore have a f^4 frequency dependence. Based on Faran's prediction of scattering of solid microspheres of this size in the frequency range of 3–8 MHz (-12 dB range of this system), the logarithm of the BSC of this phantom had a linear frequency dependence of 0.73 dB/Sr/cm/MHz (least squares linear fit to the BSC). The attenuation coefficient of the breast reference phantom was measured to be 0.15 dB/cm/MHz using the insertion loss technique, in which plexiglass was used as the reference material.[36] Since the phantom is relatively homogeneous, attenuation correction of the reference power spectrum is straightforward. However, since the human breast is inhomogeneous, correcting the spectra for the attenuation of intervening tissue layers in the beam propagation path would require accurate knowledge of the intervening tissue attenuation coefficients and proper segmentation of the tissue boundaries. Alternatively, a gross attenuation correction was performed using an assumed attenuation coefficient of 1 dB/cm/MHz, based on the average attenuation coefficient of breast tumors, subcutaneous fat, internal fat, and glandular parenchyma, obtained from findings in the literature.[37] Once the BSC estimate of a ROI in the sample was obtained, the average ESD and EAC for the ROI were estimated by least

squares fitting of the estimated and theoretical BSCs, as described by Insana and Hall.[38] For the theoretical BSC, both the Gaussian and the Anderson form factors were initially considered.[33,39] The Gaussian form factor describes spherical scatterers whose acoustic impedance vary continuously (Gaussian) with the surrounding material, while the Anderson form factor describes scattering from fluid-filled spheres. After comparing the ESD and EAC estimates obtained from the two models in limited data, the results demonstrated that there was no statistically significant difference between the values estimated from the two models. Thus, we chose the Gaussian form factor for tissue characterization in this study because on average it provided a better fit to the measured BSC (higher r^2 value) across the frequency bandwidth, and the model computation time was considerably shorter. In contrast to the SAS estimation which is based on detection of coherent scatterers, the Gaussian form factor is a model for estimating the properties of incoherent scatterers. The scatterer size and acoustic concentration parameters estimated from this form factor have been proven useful for characterizing mouse models of breast cancer and human lymph nodes.[5,12]

2.E. Statistical analysis

Statistical tests were used to compare the tumor and normal tissue groups, and tumor subtypes, in terms of the means of QUS parametric maps. Throughout the rest of the paper, the term "mean QUS value" will be used to refer to the mean of the parametric map of a QUS parameter. To determine the type of statistical test to use to compare the groups, a Shapiro-Wilk normality test was performed on each parametric data set to determine whether it follows a normal distribution. For the data sets that passed the normality test, unpaired t-tests were used to compare tumor with normal tissue. Otherwise, Mann-Whitney unpaired test was used. Additionally, pairwise comparisons were performed on tumors and normal tissues using paired t-test for normally distributed data, and Wilcoxon paired test on nonparametric data. For comparison of tumor grades, a one-way ANOVA was performed for datasets that passed the normality test, otherwise, the Kruskal-Wallis test was used. A 95% confidence interval was used in all cases. For those QUS parameters whose absolute means were poorly separable, the mean QUS value of each subject was normalized to its corresponding mean normal tissue QUS value, to improve the class separation (paired difference, denoted as ΔQUS). This normalization was necessary for MBF, SS, SI, and SAS, while the absolute tumor values for ESD and EAC were sufficient to obtain statistically significant results. The significance of performing such normalization is that there are inherent variations in echogenecity levels among patients and tumors which cannot be eliminated by calibration to a reference phantom. Patient background ultrasound backscatter can vary by patient age, menstrual cycle phase, and breast density. For comparison of parameters affected by echogenecity (i.e., SS, MBF, and SI), subtracting away the corresponding normal tissue echogenecity helps normalize such interpatient variations. This also paves the way for comparing one

patient against data obtained at a future time (intrapatient variations).

Moreover, higher order statistical features of the parametric maps of tumors were extracted by a texture analysis technique utilizing the Grey Level Co-occurrence Matrix (GLCM) computed from parametric maps. GLCMs characterize the texture of an image by describing how often certain pairs of pixels occur in the image in a specified spatial relationship. The concept of GLCMs for image classification have been described in more detail elsewhere.[40] The features that were extracted from the GLCM of each parametric map were, contrast (CON), correlation (COR), homogeneity (HOM), and energy (ENE), as defined in Ref. 40.

3. RESULTS

3.A. Patient characteristics

Relevant patient characteristics, including age, tumor size, tumor type, grade, and hormone receptor expressions (ER/PR/HER2), are summarized in Table I. The patients had an average age of 49 (SD = 11) with mean size (longest diameter) of 7.5 cm (SD = 4 cm). Tumors were predominantly of the invasive ductal carcinoma type (98%), with the exception of one case of invasive micropapillary carcinoma. The tumors were largely grade II (N = 19) or III (N = 19), with a few incidences of grade I (N = 4). Six patients had triple negative breast cancer, and the rest had at least one positive receptor expression.

3.B. Quantitative ultrasound results

Mean QUS values for each patient were obtained for both tumor and normal breast tissue. Mean normalized power spectra for normal tissue, grade I, II, and III tumors corresponding to all patients in each group are presented in Fig. 1. Nested averaging was performed to obtain the curves in Fig. 1—averaging the window spectra to obtain the ROI
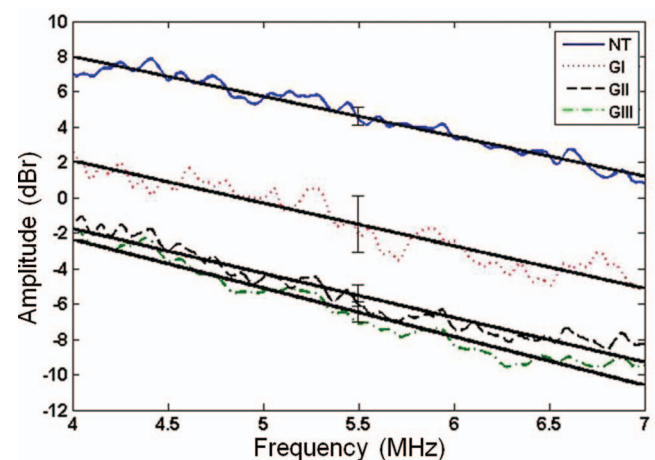

FIG. 1. Mean normalized spectral plots of normal tissue (NT, N = 42), grade I (GI, N = 4), grade II (GII, N = 19), and grade III (GIII, N = 19) tumors over all the patients in each group with corresponding lines of best fit and standard error of the MBF.
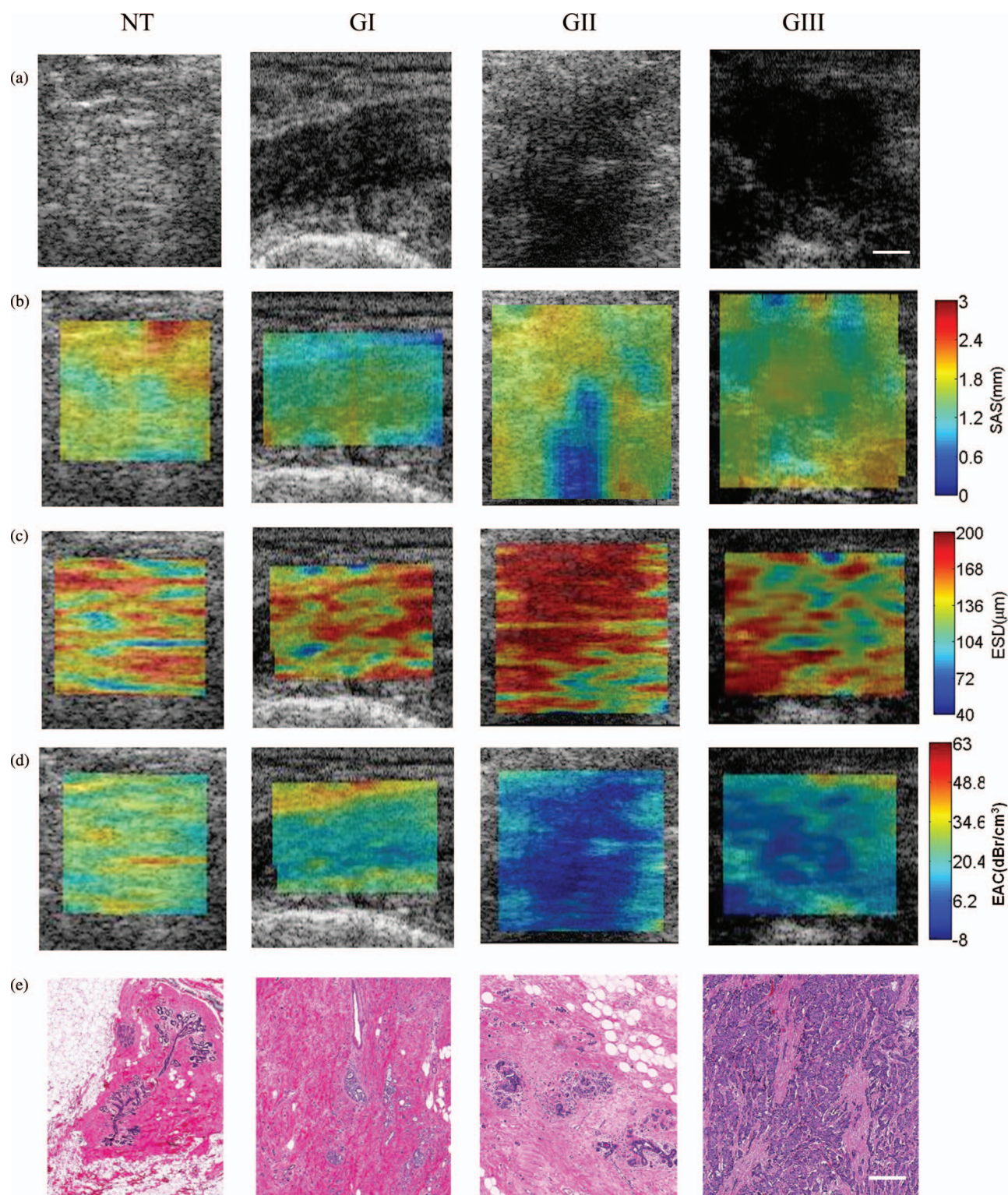
FIG. 2. B-mode images (a) and corresponding SAS maps (b), ESD maps (c), EAC maps (d), and H and E histology images (e) of typical normal breast tissue, grade I, grade II, and grade III tumors from left to right. Scale bars: 1 cm (US), 100 μm (histology).

spectrum, then averaging the ROI spectra across all patients in each group to obtain the mean spectrum for each tissue class. The plots indicate that the MBF and SI decrease from normal tissue to tumor and continue descent with increasing grade, while the SS parameter does not change considerably.

B-mode images of sample normal tissue, grade I, II, and III tumors along with the parametric maps of SAS, ESD, and EAC, are presented in Figs. 2(a)–2(d). In the SAS maps, tumors seemed to differ in the degree of heterogeneity according to tumor grade while the normal tissue was characterized by a much more heterogeneous and larger SAS. On

the other hand, ESD maps did not aid in differentiating tumor types and depicted both tumors and normal tissues as relatively heterogeneous structures. Nevertheless, the grade II tumors tend to present a higher overall ESD compared to grade III. EAC tumor maps appeared to present homogeneity with indiscriminate features, while the normal tissue tended to present more heterogeneity with a higher mean value. Figure 2(e) presents representative hematoxylin and eosin histology sections of normal tissue and tumors of grade I, II, and III, respectively. In the histology images, the normal tissue is comprised of microlobules (purple stained) surrounded by stroma (pink stained) and fat (white). Tumor histology images depicted cancerous tissue with increasingly disordered glandular structures and decreasing stromal content with increasing tumor grade. Visual examination of the mammary glands in the tumors and microlobules in the normal breast tissues revealed sizes of 100 ± 10 and 114 ± 8 μm, respectively. In comparison, mean ESDs corresponding to the tumor and normal breast tissue were determined to be 149 ± 11 and 143 ± 14 μm, respectively.

3.C. Statistical QUS analysis of cancerous versus normal tissue

One-dimensional (1D) scatter plots of MBF, SS, SI, SAS, ESD, and EAC are presented in Fig. 3. For MBF and ESD, paired/unpaired t-tests were performed between the tumor and normal tissue groups, since the data passed the normality test. For SS, SI, SAS, and EAC, Wilcoxon/Mann-Whitney

TABLE II. Classifier performances using different combinations of advanced QUS parameters for tumor versus normal tissue classification—(ESD, EAC), (ESD, SAS), (EAC, SAS), and (ESD, EAC, SAS). AUC—area under the ROC curve.

	ESD, EAC	ESD, SAS	EAC, SAS	ESD, EAC, SAS
Accuracy (%)	78	68	82	83
Sensitivity (%)	88	56	86	88
Specificity (%)	81	91	91	91
AUC	0.92	0.82	0.96	0.96

(paired/unpaired) tests were performed to account for the non-normal distributions. These tests resulted in (paired, unpaired) p-values of <0.0001, 0.0001* (MBF), 0.0075, 0.038* (SS), 0.0001, 0.0008* (SI), <0.0001, 0.0001* (SAS), 0.0042, 0.0279* (ESD), and <0.0001, 0.0001* (EAC), comparing tumor to normal tissue. All six parameters demonstrated statistically significant different means ($p < 0.05$) between tumor and normal tissue, both in paired and unpaired terms. In terms of class separation, however, there was a large overlap of the distributions of the QUS parameters. To improve the class separation, we performed multivariate statistical analysis using the quadratic discriminant function. Combinations of ESD, EAC, and SAS were tested, since these QUS parameters provide useful physical insight about tissue microstructure and their means were found to be statistically different in tumors versus normal tissue. Classification performance results demonstrated sensitivity and specificity reaching as high as 88% and 91%, using the combination of (ESD, EAC, SAS). Classification results using combinations of (ESD, EAC), (ESD, SAS), (EAC, SAS), and (ESD, EAC, SAS) are summarized in Table II. Listed are four performance measures including accuracy, sensitivity, specificity, and area under the receiver operator characteristic (ROC) curve (AUC). This table summarizes the accuracy of the classifier in correctly classifying tumors and normal tissues based on the mean QUS values. Here, the true labels for tumors were determined from the biopsy-proven tumor location. Normal tissue labels were determined from the B-mode images as they are rather obvious to the naked eye and the selected image plane was distant from the biopsy-proven tumor location. The ROC analysis results suggest that the combination (ESD, SAS) perform the poorest and (ESD, EAC, SAS) provides the highest accuracy, sensitivity, and specificity combination, slightly outperforming the (EAC, SAS) combination in terms of accuracy (1%). A 2D scatter plot of the best pairwise combination, (EAC, SAS), including the quadratic curve that best divides the classes are presented in Fig. 4. This plot illustrates an improved class separation with QUS combinations compared to single QUS parameters (Fig. 3) for tumor versus normal tissue classification. The ROC curves for (ESD, EAC), (ESD, SAS), (EAC, SAS), and (ESD, EAC, SAS) combinations are presented in Fig. 5. As evident from the figure, the combinations (EAC, SAS) and (EAC, ESD, SAS) yield curves closest to the top left corner position, indicating optimal sensitivity/specificity pairs, and the largest AUCs.
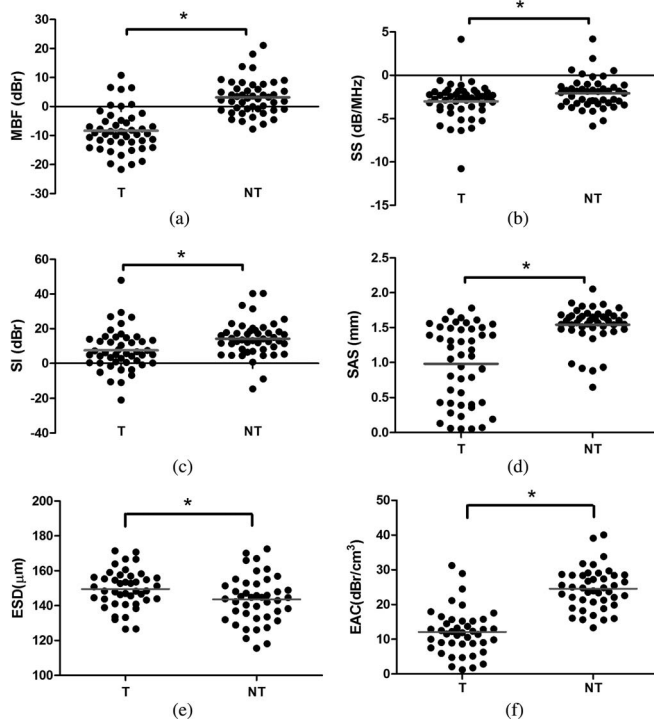

FIG. 3. Scatter plots of MBF (a), SS (b), SI (c), SAS (d), ESD (e), and EAC (f) versus tissue class (tumor or normal tissue) with the means shown by the horizontal line. T refers to tumor and NT refers to normal tissue. The mean of each group is represented by the horizontal line.
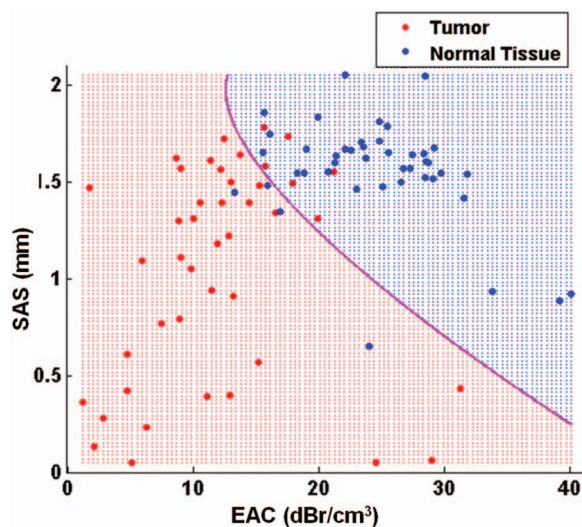
FIG. 4. 2D scatter plot of SAS versus EAC of tumors and normal tissues. The class dividing curve represents the quadratic discriminant function.

3.D. Statistical QUS analysis of tumor grade

1D scatter plots of the QUS parameters corresponding to the three tumor grades are presented in Figs. 6(a)–6(f). All QUS parameters passed the Shapiro-Wilk normality test and thus, one-way ANOVA tests were performed to compare the means of the QUS parameters across the grades. One-way ANOVA testing resulted in p-values of 0.51 (ΔMBF), 0.38 (ΔSS), 0.19 (ΔSI), 0.014* (ΔSAS), 0.035* (ESD), and 0.80 (EAC). Textural analysis was consequently performed on the ESD and SAS maps, whose means demonstrated significant ANOVA p-values. Among the four texture-based parameters investigated (CON, COR, HOM, ENE), none demonstrated a statistically significant difference among tumor grades alone. However, after applying linear discriminant classification on the input combination of all texture-based parameters as well as the mean of the ESD maps, the resulting function pro-

vided a highly statistically significant difference among tumor grades (ANOVA p-value = 0.004**). Statistical difference did not improve for the SAS parameter when its texture-based parameters were combined with its mean (ANOVA p-value of 0.077). A 1D scatter plot of this linear discriminant function of the ESD mean combined with texture-based parameters of the ESD maps is shown in Fig. 6(g). The results of ANOVA and *post hoc* analyses on ΔSAS mean, SAS mean plus texture-based parameters, ESD mean, and ESD mean plus texture-based parameters are summarized in Table III.

4. DISCUSSION

Previous QUS tissue characterization studies have primarily focused on discerning malignant masses from benign masses in preclinical tumor models. This study investigated the QUS characteristics of normal breast tissue and tumor subtypes (grades) in LABC patients. The breast tumor versus normal breast tissue characterization results in this study are in keeping in general with previous findings in spectral-analysis based prostate cancer and cancerous lymph node characterizations.[11, 12] Those studies primarily determined QUS differences associated with malignant cells. In the prostate study, lower MBF levels were associated with prostate cancer compared to that of benign prostate hyperplasia or normal prostate glands. Similarly here, we obtained lower MBF levels within tumors compared to normal breast tissue. Also, cancer-filled lymph nodes were found to exhibit lower EAC levels compared to noncancerous lymph nodes, which is also consistent with the EAC findings in this study. Previous *in vivo* studies by Oelze *et al.* on the QUS based differentiation of rat mammary fibroadenoma versus 4T1 mouse carcinoma,[5] and mammary carcinoma versus sarcoma,[7] demonstrated significant differences in the EAC between the different tissue types. This suggests that the spatial organization of cells (and larger structures such as glandular acini) may play an important role in the differentiation of these tissue types. Likewise, the histological data here show that normal breast tissues have much more organized microstructure compared to that of tumors, which likely contributed to the differences in the EAC that were observed.

A similar study which attempted to use QUS techniques to characterize clinical breast masses (benign versus malignant masses) in terms of attenuation, ESD, and heterogeneity index, found subtle differences in these parameters between the breast masses.[8] This was not surprising as our study found that coherent scattering parameters (i.e., SAS) and incoherent scattering parameters (i.e., ESD and EAC) provide complimentary information about a breast tumor which differentiates it from its surrounding (but not adjacent) tissues. However, their study did not include analysis of incoherent scattering properties of breast masses or higher order spacing such as that investigated here which provided additional tissue characterization features.

The spectral plots presented in Fig. 1 were obtained from relatively large regions of tumors (up to 5×5 cm) which include tumor heterogeneity. However, as a result of averaging the individual line spectra over the tumor region,
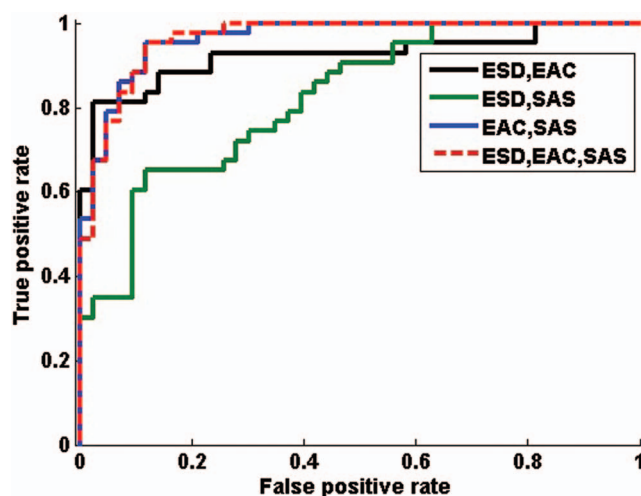

FIG. 5. ROC curves for the classifier trained using advanced QUS parameters including (ESD, SAS), (ESD, EAC), (EAC, SAS), and (ESD, EAC, SAS). All samples were used to train and test the classifier.
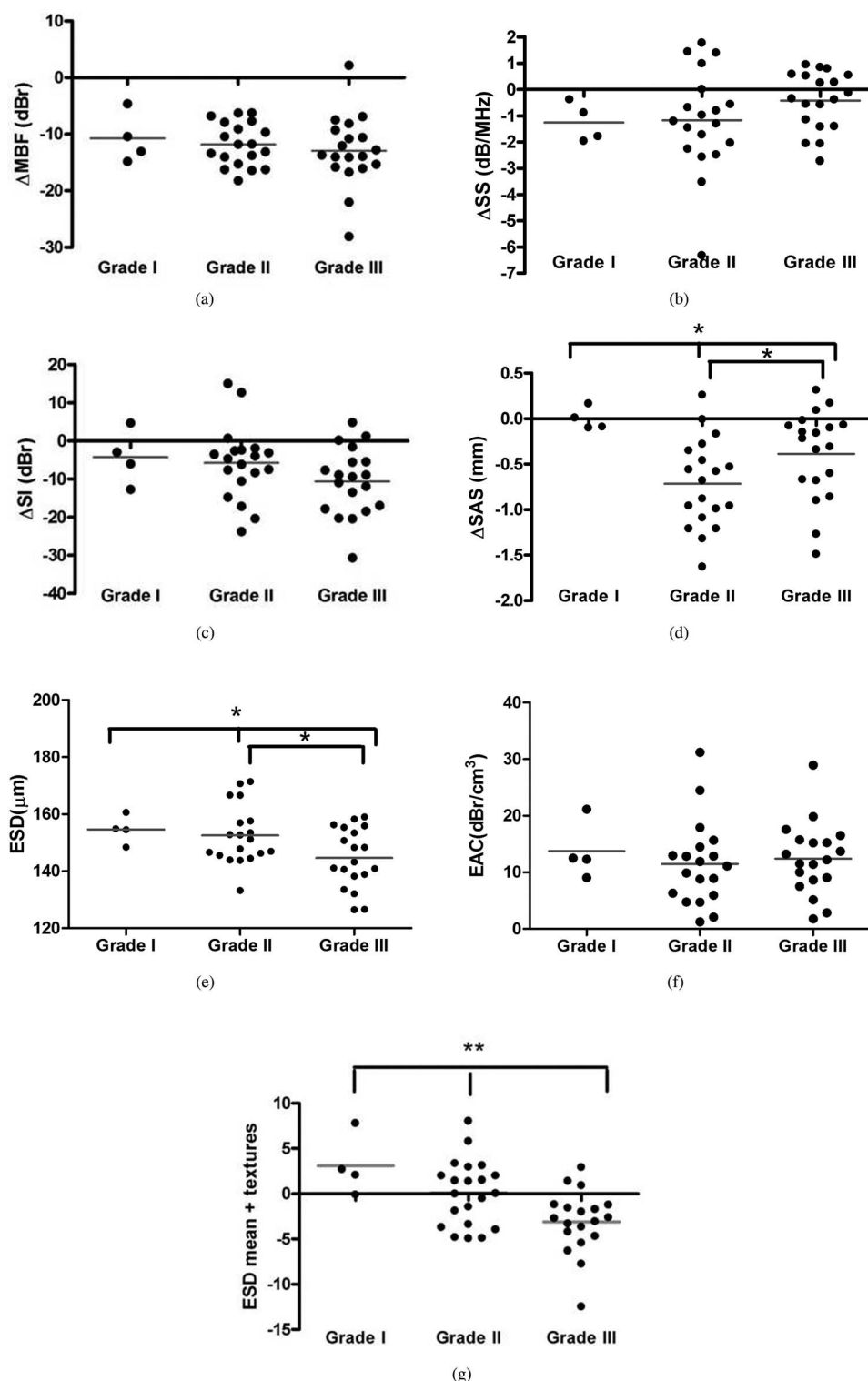
FIG. 6. Scatter plots of the four QUS parameters MBF (a), SS (b), SI (c), SAS (d), ESD (e), and EAC (f), versus tumor grade, showing the mean with a horizontal line. (g) Linear discriminant function of the mean of ESD combined with CON, CORR, HOM, and ENE parameters. The asterisk indicates statistically different means based on ANOVA test (* = p < 0.05, ** = p < 0.005).

information about the heterogeneity of the tumors was lost. The poor separability of grade II and III tumors based on their spectral characteristics is perhaps due to this averaging. One can observe that including texture-based statistical parameters, such as homogeneity [Fig. 6(g)], can improve

separability of tissues whose differences arise mainly from the degree of heterogeneity. We anticipate that the spectral plots presented in Fig. 1 may be a way to quantitatively describe the "echo pattern" that contributes to the BIRADS readings, although this is untested and would be the subject of

TABLE III. Table of p-values of significance of the following parameters/parameter combinations demonstrating statistically different means among tumor grades: ΔSAS mean, SAS mean plus textures, ESD mean, and ESD mean plus textures.

		ΔSAS	SAS mean + textures	ESD mean	ESD mean + textures
	ANOVA	0.014[a]	0.077	0.035[a]	0.004[b]
Post-test	GI vs GII	0.009[a]	0.147	0.708	0.046[a]
	GI vs GIII	0.140	0.060	0.079	0.001[b]
	GII vs GIII	0.044[a]	0.186	0.023[a]	0.056

[a]p-value < 0.05.
[b]p-value < 0.005.

potential future investigation. Another point to note in Fig. 1 is that the normalized power spectrum was used for the vertical axis, rather than the BSC. Although the BSC has been demonstrated to be instrument-independent and reproducible across ultrasound platforms in the literature,[35] when we attempted to plot the BSC in a similar manner as Fig. 1, the separation of the tissue classes was poorer and there was no consistent trend. Like the normalized power spectra, the following order in the BSC magnitude was expected from lowest to highest: GIII, GII, GI, NT, but this trend was not observable with the BSC. This is due potentially to the fact that an accurate representation of the BSC requires attenuation to be taken into account, which, in the case of a breast, is complex. It is possible that the uniform attenuation assumption used in this study resulted in relatively poor separability of the tissue types in terms of the BSC, compared to what would occur having an accurate knowledge of intervening tissue attenuation. Spectral-based attenuation estimation methods have been proposed in the literature, but such methods have limitations such as homogeneous ROI requirement (no variations in scatterer size).[41] Nevertheless, a normalized log power spectrum is an alternative system-independent parameter. Normalizing the sample power spectrum to that of a well-characterized reference phantom (characterized in terms of attenuation, BSC, and scatterer size) removes the system transfer function as well as diffraction effects.

The linear regression spectral parameters determined here demonstrated statistically different means in tumors and normal tissues (p < 0.04), but failed to do so in tumor grades. Although normalization to normal tissue improved the separation marginally, the means of the normalized values (ΔMBF, ΔSS, ΔSI) were still not statistically different among tumor grades. In contrast, the ΔSAS parameter demonstrated statistically significant difference among tumor grades (p = 0.014 while also showing contrast with normal tissue (p-values <0.001). Although there is a considerable spread in the QUS values within a normal tissue ROI, the mean value served as a good normalization metric, as it normalized out the differences in the inherent echogenecity levels of different breasts (due to different attenuation properties). Standardizing the selection of a normal breast tissue region in an ultrasound image is a clinically challenging task. As

such, where possible, absolute values of the mean QUS parameters were used for classification. It is important to note that, due to the large number of observations (N), p-values are not definitive measures of group separation. For this reason, discriminant analysis was performed in addition to statistical tests to obtain a more definitive measure of group separation.

The speed of sound and attenuation properties of the different components of the breast are important for SAS and spectral analysis. The speed of sound values assumed for computing SAS, 1455 m/s for normal tissue and 1540 for tumor, were based on reported *in vivo* ultrasound tomography measurements of the fat and parenchyma (1422 ± 9, 1487 ± 21 m/s, respectively), and malignant masses (1548 ± 17 m/s) in the breast. These values fell in the same range as the *ex vivo* measurements of normal breast tissue (fat and parenchyma) which ranged from 1400 to 1540 m/s and those of tumors which ranged from 1500 to 1600 m/s.[42] Similarly, attenuation coefficient values corresponding to different structures in the breast were measured using ultrasound tomography and reported in Ref. 38. From these data, the mean attenuation coefficient of all normal structures in the breast and a typical breast tumor, in estimation calculates to 0.98 ± 0.49 dB/cm MHz, which was rounded to 1 dB/cm MHz in this work. As evident, there are variations in the attenuation coefficient of different structures in the breast and among patients. Tumors of different grades may also have different attenuation properties. This is important in tissue characterization since QUS parameters can be influenced by attenuation. However, a value of 1 dB/cm MHz was used as a reasonable approximation for an intermediate calculation parameter and for this first technical report on tumor grade characterization.

As discussed, many patient-specific factors can contribute to the variability in QUS measurements observed, including age, menstrual cycle phase, breast density, and tumor receptor expressions, some of which have been identified in Table I. Another feature that may confound QUS measurements of breast tumors is the extent of ductal carcinoma *in situ*, which describes the portion of the overall tumor volume that is noninvasive. However, the extent of this effect is currently not known and will be dealt with elsewhere upon further investigation.

The ESD estimation in breast tumors and normal breast tissues aided in identifying the structures potentially responsible for ultrasound scattering at clinically relevant frequencies. Particularly, ESD estimates in tumors (149 ± 11 μm) generally corresponded on the same order of magnitude to the mean size of the glands seen in tumor histology (100 ± 10 μm). Perfect correspondence was not expected as QUS measures the properties of "effective" scatterers and there are many scatterers of different sizes corresponding to different microstructures in the breast. However, tissue characterization of the breast was found to be more successful when the ESD parameter was combined with parameters describing the spatial organization of the tissue microstructure (i.e., EAC and SAS).

Parametric maps of normal breast tissues and different tumors demonstrated patterns which reflected their microstructural properties seen grossly in the histology. For instance,

the SAS maps of normal tissues presented a larger mean SAS compared to tumors. Interestingly, the SAS maps of the grade I tumor appeared indistinguishable from its surrounding tissue. This is not surprising as a grade I tumor consists of well-differentiated cells, possessing microstructural properties similar to those of a normal breast tissue. The abrupt variations in SAS of the grade II tumor can be related to the patchiness of glands, as evident in the histology. In contrast, the grade III tumors presented a degree of randomness in the SAS, which is consistent with the dominant and disordered organization of the glands as evident in histology.

The ESD maps seem to be useful tools for distinguishing tumor grades and normal breast tissues. The distinction arises likely from their texture. Specifically, grade I tumors show multiple patches of small ESDs ($\sim$136 μm), surrounded by a background of large ESDs ($\sim$200 μm). This is similar to the islands of small glands ($\sim$100 μm) surrounded by the stroma in the histology. On the other hand, the grade II tumor presents mostly homogeneous and large ESDs ($\sim$200 μm). This can be explained by histology which demonstrates enlarged glands which have invaded nearly 50% of the stromal space. Finally, the ESDs in the grade III tumor presents a similar pattern to that of grade I tumor (patches of small ESDs surrounded by large ESD background). At this tumor grade, since glands occupy the majority of the space, the stroma are thought to be the scatterers that the ESD map is depicting. However, there is an ambiguity in the classification of grade I and III tumors only on the basis of ESD maps, as the type of scatterers (stroma or glands) cannot be differentiated at this frequency range ($\sim$ 6 MHz). The EAC maps, on the other hand, fail to provide information about tumor grade, but clearly separate normal tissue from tumors. The EAC proved to be more powerful at tumor versus normal tissue classification when statistically combined with SAS. This further supported the suggestion that the coherent and incoherent scattering properties of breast tumors are uncorrelated and are the basis for differentiation of tumor versus normal tissue.

Multiparametric analysis of tumor grades using combinations of mean QUS parameters did not improve grade discrimination. However, the nature of the parametric maps of tumors was suggestive of textural differences between tumors. Thus, texture-based parameters extracted from the parametric maps were investigated for differentiating tumor grades. Texture analysis demonstrated that measures of textural variations in the ESD maps, when combined with the mean, provided more discriminative information about tumor grades.

In summary, multiparametric analysis of advanced scattering parameters extracted from the RF ultrasound signal backscattered from breast tumors can sensitively (88%) and specifically (91%) distinguish tumors from proximal normal breast tissue. Furthermore, textural features, combined with the means of parametric maps of breast tumors proved to be potentially useful in characterizing breast tumors in terms of their histological grade. The method proposed here provides objective characterization of breast tumors, providing separation from normal breast tissue and providing grade-linked microstructural information.

[a] Author to whom correspondence should be addressed. Electronic mail: Gregory.Czarnota@sunnybrook.ca; Telephone: 416-480-6100 $\times$ 7073; Fax: 416-480-6002.

[1] S. H. Giordano, "Update on locally advanced breast cancer," Oncologist **8**, 521–530 (2003).

[2] *Guidelines for the Management of Breast Cancer*, 31st ed., EMRO Technical Publications Series (World Health Organization, Alexandria, Egypt, 2006), p. 44.

[3] J. H. Youk, E.-K. Kim, M. J. Kim, J. Y. Lee, and K. K. Oh, "Missed breast cancers at US-guided core needle biopsy: How to reduce them," Radiographics **27**, 79–94 (2007).

[4] M. Insana and M. Oelze, "Advanced ultrasonic imaging techniques for breast cancer research," *Emerging Technologies in Breast Imaging and Mammography* (American Scientific Publishers, Valencia, CA, 2006).

[5] M. L. Oelze, W. D. O' Brien, J. P. Blue, and J. F. Zachary, "Differentiation and characterization of rat mammary fibroadenomas and 4T1 mouse carcinomas using quantitative ultrasound imaging," IEEE Trans. Med. Imaging **23**, 764–771 (2004).

[6] E. J. Feleppa, J. Mamou, C. R. Porter, and J. Machi, "Quantitative ultrasound in cancer imaging," Semin. Oncol. **38**, 136–150 (2011).

[7] M. L. Oelze and J. F. Zachary, "Examination of cancer in mouse models using high-frequency quantitative ultrasound," Ultrasound Med. Biol. **32**, 1639–1648 (2006).

[8] H. Nasief, I. Rosado-Mendez, J. Zagzebski, and T. Hall, "Quantitative ultrasound as an aid to differentiate benign from malignant breast masses," in *AIUM (American Institute of Ultrasound in Medicine) Annual Convention*, New York, NY, 2013.

[9] F. L. Lizzi, M. Ostromogilsky, E. J. Feleppa, M. C. Rorke, and M. M. Yaremko, "Relationship of ultrasonic spectral parameters to features of tissue microstructure," IEEE Trans. Ultrason. Ferroelectr. Freq. Control **34**, 319–329 (1987).

[10] D. J. Coleman, F. L. Lizzi, R. H. Silverman, L. Helson, J. H. Torpey, and M. J. Rondeau, "A model for acoustic characterization of intraocular tumors," Invest. Ophthalmol. Visual Sci. **26**, 545–550 (1985).

[11] E. J. Feleppa, A. Kalisz, J. B. Sokil-Melgar, F. L. Lizzi, A. L. Rosado, M. C. Shao, W. R. Fair, M. S. Cookson, V. E. Reuter, and W. D. W. Heston, "Typing of prostate tissue by ultrasonic spectrum analysis," IEEE Trans. Ultrason. Ferroelectr. Freq. Control **43**, 609–619 (1996).

[12] J. Mamou, A. Coron, M. Hata, J. Machi, E. Yanagihara, P. Laugier, and E. J. Feleppa, "Three-dimensional high-frequency characterization of cancerous lymph nodes," Ultrasound Med. Biol. **36**, 361–375 (2010).

[13] M. Yang, T. M. Krueger, J. G. Miller, and M. R. Holland, "Characterization of anisotropic myocardial backscatter using spectral slope, intercept and midband fit parameters," Ultrason. Imaging **29**, 122–134 (2007).

[14] F. L. Lizzi, M. Astor, T. Liu, C. Deng, D. J. Coleman, and R. H. Silverman, "Ultrasonic spectrum analysis for tissue assays and therapy evaluation," Int. J. Imaging Syst. Technol. **8**, 3–10 (1997).

[15] R. M. Vlad *et al.*, "Quantitative ultrasound characterization of responses to radiotherapy in cancer mouse models," Clin. Cancer Res. **15**(6), 2067–2074 (2009).

[16] J. Lee, R. Karshafian, N. Papanicolau, A. Giles, M. C. Kolios, and G. J. Czarnota, "Quantitative ultrasound for the monitoring of novel microbubble and ultrasound radiosensitization," Ultrasound Med. Biol. **38**, 1212–1221 (2012).

[17] L. L. Fellingham and F. G. Sommer, "Ultrasonic characterization of tissue structure in the *in vivo* human liver and spleen," IEEE Trans. Sonics Ultrason. **31**, 418–428 (1984).

[18] K. Suzuki, N. Hayashi, Y. Sasaki, M. Kono, A. Kasahara, Y. Imai, H. Fusamoto, and T. Kamada, "Evaluation of structural change in diffuse liver disease with frequency domain analysis of ultrasound," Hepatology **17**, 1041–1046 (1993).

[19] C. B. Machado, W. C. Pereira, M. Meziri, and P. Laugier, "Characterization of *in vitro* healthy and pathological human liver tissue periodicity using backscattered ultrasound signals," Ultrasound Med. Biol. **32**, 649–657 (2006).

[20] U. Abeyratne and X. Tang, "Ultrasound scatter-spacing based diagnosis of focal diseases of the liver," Biomed. Signal Process. Control **2**, 9–15 (2007).

[21] Y. Bige, Z. Hanfeng, and W. Rong, "Analysis of microstructural alterations of normal and pathological breast tissue *in vivo* using the AR cepstrum," Ultrasonics **44**, 211–215 (2006).

[22] K. A. Wear, R. F. Wagner, M. F. Insana, and T. J. Hall, "Application of autoregressive spectral analysis to cepstral estimation of mean scatterer spacing," IEEE Trans. Ultrason. Ferroelectr. Freq. Control **40**, 50–58 (1993).

[23] X. Tang and U. R. Abeyratne, "Wavelet transforms in estimating scatterer spacing from ultrasound echoes," Ultrasonics **38**, 688–692 (2000).

[24] J. Tsao and G.-S. Jiang, "Mean scatterer spacing estimation using wavelet spectrum," Proc.-IEEE Ultrason. Symp. **3**, 2090–2093 (2004).

[25] T. Varghese and K. D. Donohue, "Characterization of tissue microstructure scatterer distribution with spectral correlation," Ultrason. Imaging **15**, 238–254 (1993).

[26] Y.-Y. Liao, P.-H. Tsui, C.-H. Li, K.-J. Chang, W.-H. Kuo, C.-C. Chang, and C.-K. Yeh, "Classification of scattering media within benign and malignant breast tumors based on ultrasound texture-feature-based and Nakagami-parameter images," Med. Phys. **38**, 2198–2207 (2011).

[27] S. H. Kim, B. K. Seo, J. Lee, S. J. Kim, K. R. Cho, K. Y. Lee, B.-K. Je, H. Y. Kim, Y.-S. Kim, and J.-H. Lee, "Correlation of ultrasound findings with histology, tumor grade, and biological markers in breast cancer," Acta Oncol. **47**, 1531–1538 (2008).

[28] H. J. Bloom and W. W. Richardson, "Histological grading and prognosis in breast cancer: A study of 1409 cases of which 359 have been followed for 15 years," Br. J. Cancer **11**, 359–377 (1957).

[29] K. A. Topp, J. F. Zachary, and W. D. O'Brien, "Quantifying B-mode images of *in vivo* rat mammary tumors by the frequency dependence of backscatter," J. Ultrasound Med. **20**, 605–612 (2001).

[30] E. L. Madsen, J. A. Zagzebski, R. A. Banjavie, and R. E. Jutila, "Tissue mimicking materials for ultrasound phantoms," Med. Phys. **5**, 391–394 (1978).

[31] S. M. Kay, *Modern Spectral Estimation: Theory and Application* (Prentice-Hall, Englewood Cliffs, NJ, 1998).

[32] C. Li, N. Duric, P. Littrup, and L. Huang, "*In vivo* breast sound-speed imaging with ultrasound tomography," Ultrasound Med. Biol. **35**, 1615–1628 (2009).

[33] M. F. Insana, R. F. Wagner, D. G. Brown, and T. J. Hall, "Describing small-scale structure in random media using pulse-echo ultrasound," J. Acoust. Soc. Am. **87**, 179–192 (1990).

[34] L. X. Yao, J. A. Zagzebski, and E. L. Madsen, "Backscatter coefficient measurements using a reference phantom to extract depth-dependent instrumentation factors," Ultrason. Imaging **12**, 58–70 (1990).

[35] J. J. Anderson, M. Herd, M. R. King, A. Haak, Z. T. Hafez, J. Song, M. L. Oelze, E. L. Madsen, J. Zagzebski, W. D. O'Brien, and T. J. Hall, "Interlaboratory comparison of backscatter coefficient estimates for tissue-mimicking phantoms," Ultrason. Imaging **32**, 48–64 (2010).

[36] F. T. D'Astous and F. S. Foster, "Frequency dependence of ultrasound attenuation and backscatter in breast tissue," Ultrasound Med. Biol. **12**(10), 795–808 (1986).

[37] N. Duric, P. Littrup, A. Babkin, D. Chambers, S. Azevedo, A. Kalinin, R. Pevzner, M. Tokarev, E. Holsapple, O. Rama, and R. Duncan, "Development of ultrasound tomography for breast imaging: Technical assessment," Med. Phys. **32**, 1375–1386 (2005).

[38] M. F. Insana and T. J. Hall, "Parametric ultrasound imaging from backscatter coefficient measurements: Image formation and interpretation," Ultrason. Imaging **12**, 245–267 (1990).

[39] V. C. Anderson, "Sound scattering from a fluid sphere," J. Acoust. Soc. Am. **22**, 426–431 (1950).

[40] R. M. Haralick, K. Shanmugam, and I. Dinstein, "Textural features for image classification," IEEE Trans. Syst. Man Cybern. **3**, 610–621 (1973).

[41] Y. Labyed and T. A. Bigelow, "A theoretical comparison of attenuation measurement techniques from backscattered ultrasound echoes," J. Acoust. Soc. Am. **129**, 2316–2324 (2011).

[42] P. D. Edmonds, C. L. Mortensen, J. R. Hill, S. K. Holland, J. F. Jensen, P. Schattner, and A. D. Valdes, "Ultrasound tissue characterization of breast biopsy specimens," Ultrason. Imaging **13**, 162–185 (1991).